ENTROPY AND ENERGY MEASURES: COMPLEMENTARY TOOLS FOR ANALYZING REACTION DIFFUSION DYNAMICS*

OWEN SKRILOFF†

Abstract. Reaction diffusion systems exhibit rich dynamical behaviors, including emergent pattern formation, phase transitions, and applications across science and engineering. This study evaluates the effectiveness of two well-documented measures for characterizing system dynamics: Shannon entropy, a statistical measure of information uncertainty, and the energy norm, a physical metric capturing both local and global deviations. A coupled reaction diffusion problem was solved across a range of diffusivity and reactivity parameters, producing solutions with diverse dynamical behaviors. Analysis of these solutions using both measures reveals their complementary strengths. The entropy measure excels in detecting sharp phase boundaries with minimal time data, while the energy norm provides detailed insights into subtle variations within dynamic regimes. These findings underscore the utility of combining these measures to achieve a comprehensive understanding of reaction diffusion dynamics.

1. Introduction. Phase transitions and criticality are central to understanding the emergent behavior of dynamical systems, appearing in a wide range of fields such as stochastic processes, data science, biological systems, and of course, statistical mechanics and thermodynamics. Historically, phase transitions have been studied through the lens of statistical mechanical thermodynamic models [1], where the system behavior is described by entropy S, energy E, and temperature T [2]. The interplay between these three quantities determines the systems evolution towards an equilibrium state x^* minimizing free energy G,

$$x^* = \text{argmin}_x\{G(x) = E(x) - TS(x)\}.$$

The dynamics of this system are widely applicable, and have been expanded beyond thermodynamics to information theory and complex systems analysis. Dynamics like those of energy and entropy often undergo phase transitions when the weighting parameter (temperature) of the two forces (energy and entropy) changes [3]. While temperature determines the phase, entropy is an excellent measure of phase changes, as sharp entropy gradients characterize critical points where emergent behavior changes [4]. Shannon entropy was originally introduced to quantify information uncertainty [5]. The generalization of entropy enabled applications in fields besides thermodynamics including data analysis and machine learning, file compression and transfer, quantum computing, and dynamical systems [6].

In dynamical systems, another approach to characterizing dynamic behavior has been to use the energy norm. This metric is effective as it captures both global deviations (via the L^2 norm) and local variations (via the gradient norm). Variations of the energy norm have been shown to measure behavior in thermoacoustic disturbances [7], fractures and mechanical degradation [7] [8], discontinuities in waveguides [9], and isotropic elastic wavefield imaging [10]. Together, these highlight the applicability of energy norms to characterize system dynamics.

Reaction diffusion problems [4] exhibit rich phase behavior and pattern formation, and are widely studied due to their emergent phenomena [11]. Alan Turing first used a model of coupled reaction diffusion equations to show how biological patterns emerge

*Submitted for Math 250 Final Project, December 17th, 2024

†Department of Mathematics, 503 Boston Ave, Tufts University, Medford, MA 02155 (owen.skriloff@tufts.edu).

from an unstable process [12]. His research led to an understanding of how patterns such as stripes on a zebra can manifest from biochemical processes [11]. The emergent behavior of reaction diffusion systems is akin to those in thermodynamics, with sharp changes in system behavior as parameters vary.

This study will compare the effectiveness of a measure based on Shannon entropy and the energy norm in characterizing the dynamic behavior of a coupled reaction diffusion dynamical system. First, the specific reaction diffusion problem for analysis will be introduced. Second, the numerical scheme for solving the reaction diffusion problem will be outlined, and proofs of conditions required for accuracy will be presented. The energy and entropy measures will then be defined. Finally, the ability of the two measures to quantify dynamic behavior will be examined by using each to characterize the system for various points in the parameter space.

2. Problem. Consider the Schnakenberg model [13], a widely studied example of a reaction diffusion system on the square domain $\Omega = [0,3] \times [0,3]$:

$$\begin{cases} \dfrac{\partial u_1}{\partial t} = D_1 \Delta u_1 - R_1(u_1, u_2)u_1 + K_1 & \text{on } \Omega \times [0, t_{end}], \\ \dfrac{\partial u_2}{\partial t} = D_2 \Delta u_2 - R_2(u_1, u_2)u_2 + K_2 & \text{on } \Omega \times [0, t_{end}], \\ \dfrac{\partial u_i}{\partial x} = \dfrac{\partial u_i}{\partial y} = 0 & \text{on } \partial\Omega \text{ for } i = 1, 2. \end{cases}$$

Here, D_1 and D_2 represent diffusion coefficients and R_1, R_2 define the reactivity of each component. Adapting the dimensionless version of the system [11], define the R functions and K constants as follows:

$$\begin{aligned} R_1(u_1, u_2) &= \gamma - \gamma u_1 u_2, \\ R_2(u_1, u_2) &= \gamma u_1^2, \\ K_1 &= \gamma a, \\ K_2 &= \gamma b. \end{aligned}$$

The constants $a = 0.1305$ and $b = 0.7695$ were fixed according to instability conditions [14]. The initial conditions of the system were small perturbations from steady state of u_1 [15]. Steady state values were derived by setting the time derivatives to zero, and when the small Gaussian perturbation is added to u_1, the initial conditions are:

$$\begin{aligned} u_1(x, y, 0) &= a + b + 10^{-3} e^{-100\left(\left(x - \frac{3}{2}\right) + \left(\left(y - \frac{3}{2}\right)\right)\right)}, \\ u_2(x, y, 0) &= \frac{b}{(a+b)^2}. \end{aligned}$$

By then defining the diffusion ratio $d = D_2/D_1$, the dynamic behavior of the solution is characterized solely by the diffusion ratio d and the reactivity constant γ. In other words, the behavior of solutions are defined by a single point in the parameter space $(\gamma, d) \in \mathcal{P}$. In the thermodynamics analogy, this point is akin to the state variables of temperature and pressure, which characterize the equilibrium phase (emergent behavior) of the solution. As such, this study will solve the problem for a variety of points in $\mathcal{P}$ and test how Shannon entropy and the energy norm can indicate emergent properties, just like classical entropy and energy does in thermodynamics.

3. Numerical solution scheme. To solve the problem, the finite element method is used for the spatial piece, and a modified Implicit Euler two level finite difference scheme is used for the temporal component. Examine the generic reaction diffusion problem

$$\frac{\partial u}{\partial t} = D\Delta u - R(u_i)u + K,$$

where u_i are any coupled terms contributing to the reactivity term. The weak form of the reaction diffusion equation is derived by multiplying by a test function $v \in H_0^1(\Omega)$ and integrating over the domain Ω

$$\int_\Omega \frac{\partial u}{\partial t} v \,\mathrm{d}\Omega = \int_\Omega D\Delta u v \,\mathrm{d}\Omega - \int_\Omega R(u_i)uv \,\mathrm{d}\Omega + \int_\Omega Kv \,\mathrm{d}\Omega.$$

After integrating by parts, the boundary integrals cancel due to the no flux Neumann boundary conditions. This leaves the weak form as

$$\int_\Omega \frac{\partial u}{\partial t} v \,d\Omega + \int_\Omega D\nabla u \cdot \nabla v \,d\Omega + \int_\Omega R(u)uv \,d\Omega = \int_\Omega Kv \,\mathrm{d}\Omega.$$

To implement the Implicit Euler finite difference scheme for the temporal portion of the equation, approximate the temporal derivative as

$$\frac{\partial u}{\partial t} \approx \frac{u_n - u_{n-1}}{h_t},$$

where h_t is the time step size, and u_{n-1} is the previous time's solution. To maintain linearity in the spatial portion, the reactivity is based on the previous time step. Under the implicit scheme, the u functions are replaced by u_n. After multiplying through by h_t we have the final weak form of problem:

$$\int_\Omega u_n v \,d\Omega + h_t \left(\int_\Omega D\nabla u_n \cdot \nabla v \,d\Omega + \int_\Omega R(u_{i,n-1})u_n v \,d\Omega \right) = \int_\Omega u_{n-1} v \,d\Omega + \int_\Omega Kv \,\mathrm{d}\Omega.$$

Linear triangular basis elements were used to approximate the solution. Simpson's quadrature routine [16] was used to approximate the integrals of the weak form. Three quadrature points (x_q, y_q) were used for the reaction term due to its nonlinearity, with a single point used for all other integrals. Since they are time independent, mass M and diffusion D matrices were assembled and stored using the basis elements using

$$M_{i,j} = \sum_q w_q \phi_i(x_q)\phi_j(y_q),$$
$$D_{i,j} = h_t D \sum_q w_q \nabla\phi_i(x_q) \cdot \nabla\phi_j(y_q),$$

To iterate one time step, the time dependent reaction matrix $R^{(n)}$ and load vector $\mathbf{f^{(n)}}$ were assembled using the previous solutions for each coupled element of the system $u_{i,n-1}$ as follows:

$$R_{i,j}^{(n)} = \sum_q w_q R(u_{i,n-1}(x_q, y_q))\phi_i(x_q)\phi_j(y_q),$$
$$\mathbf{f}_i^{(n)} = \sum_q w_q (u_{n-1}(x_q) + K)\phi_i(x_q).$$

The resulting linear system,

$$(M + D + R^{(n)})u_n = \mathbf{f}^{(n)},$$

was solved using a python algebraic multigrid package [17]. A spatial step size $h_x = h_y = 0.06$ was used, creating a 50×50 node spatial grid on which solutions were approximated. A time step size of $h_t = 0.01$ was used to evaluate 30 time points (ending with $t = 0.3$).

3.1. Stability and convergence of solution scheme. To show convergence and stability of solutions approximated in $\mathcal{V} = H_0^1(\Omega)$, the bilinear and linear form of the weak formulation of the reaction diffusion problem will be shown to have key properties. The bilinear form a and linear form l are given by

$$\begin{aligned} a(u_n, v) &= \int_\Omega u_n v \, d\Omega + h_t \left(\int_\Omega D\nabla u_n \cdot \nabla v \, d\Omega - \int_\Omega R(u_{n-1}) u_n v \, d\Omega \right), \\ l(v) &= \int_\Omega u_{n-1} v \, d\Omega + \int_\Omega K v \, \mathrm{d}\Omega. \end{aligned}$$

PROPOSITION 3.1. *The linear functional $l(v)$ is bounded.*

Proof. To show that the linear form is bounded, find a constant $C > 0$ such that

$$|l(v)| \leq C\|v\|_{H_0^1}.$$

By the Cauchy-Schwartz inequality and the definition of the Sobolev norm,

$$\begin{aligned} \left| \int_\Omega (u_{n-1} + K) v \, d\Omega \right| &\leq \|u_{n-1} + K\|_2 \|v\|_2 \\ &\leq \|u_{n-1} + K\|_2 \left(\|v\|_2 + \|\nabla v\|_2 \right) = C\|v\|_{H_0^1} \end{aligned}$$

∎.

PROPOSITION 3.2. *The bilinear form $a(u, v)$ is continuous provided that $R(u_{i,n-1}) \leq R_{max}$ and $1 + h_t R_{max} > 0$.*

Proof. To show $a(u, v)$ is continuous, find a constant $C > 0$ such that

$$a(u, v) \leq C\|u\|_{H_0^1} \|v\|_{H_0^1}.$$

Factoring out the lower bound R_{max} and reorganizing we have

$$a(u, v) \leq (1 + h_t R_{max}) \int_\Omega uv \, d\Omega + h_t D \int_\Omega \nabla u \cdot \nabla v \, d\Omega.$$

Next, apply the Cauchy-Schwartz inequality to get

$$a(u, v) \leq (1 + h_t R_{max}) \|u_n\|_2 \|v\|_2 + h_t D \|\nabla u_n\|_2 \|\nabla v\|_2.$$

Manipulating the right hand side of the continuity condition,

$$\begin{aligned} C\|u\|_{H_0^1} \|v\|_{H_0^1} &= C \left(\|u\|_2 \|v\|_2 + \|u\|_2 \|\nabla v\|_2 + \|\nabla u\|_2 \|v\|_2 + \|\nabla u\|_2 \|\nabla v\|_2 \right), \\ &= C(\|u\|_2 \|v\|_2 + \|\nabla u\|_2 \|\nabla v\|_2) + C_2, \end{aligned}$$

where $C_2 = C(\|u\|_2 \|\nabla v\|_2 + \|\nabla u\|_2 \|v\|_2) \geq 0$. By choosing C such that

$$C \geq \max\left(1 + h_t R_{max}, h_t D\right) > 0,$$

Continuity of the bilinear form is shown with

$$a(u,v) \leq \max\left(1 + h_t R_{max}, h_t D\right)\left(\|u\|_2\|v\|_2 + \|\nabla u\|_2\|\nabla v\|_2\right) \leq C\|u\|_{H_0^1}\|v\|_{H_0^1} \quad \square$$

PROPOSITION 3.3. *The bilinear form $a(u,v)$ is coercive provided that $R_{min} \leq R(u_{n-1})$ and $1 + h_t R_{min} > 0$.*

Proof. To show that $a(u,v)$ is coercive, find a constant $C > 0$ such that

$$a(u,u) \geq C\|u\|_{H_0^1}^2.$$

Bounding the bilinear form from below using R_{min} results in

$$a(u,u) \geq (1 + h_t R_{min}) \int_\Omega u^2 \, d\Omega + h_t D \int_\Omega \nabla u^2 \, d\Omega = (1 + h_t R_{min})\|u\|_2^2 + h_t D\|\nabla u\|_2^2.$$

By choosing C such that

$$0 < C \leq \min(1 + h_t R_{min}, h_t D),$$

coercivity follows with the bound

$$a(u,u) \geq \min(1 + h_t R_{min}, h_t D)(\|u\|_2^2 + \|\nabla u\|_2^2) \geq C\|u\|_{H_0^1}^2. \quad \square$$

THEOREM 3.4. *Solutions of the reaction diffusion problem are unique and converge to the smooth solution u provided the conditions for coercivity and ellipticity are met.*

Proof. By the Lax-Milgram Theorem [18], since $a(u,v)$ is continuous and coercive and $l(v)$ is a bounded linear functional, there exists a unique $u \in \mathcal{V}$ which solves the weak form. Define $\mathcal{T}$, a piecewise linear triangular mesh on which the solution will be approximated. Since $\mathcal{T}$ is within the family of non-degenerate simplex meshes on a polyhedral domain $\Omega_h \subset R^n$, the error of the approximate solution u_h on this mesh is bounded [18]. Temporal stability follows from spatial stability, since each time step is an instance of solving the stable spatial system which depends on the previous time step. $\square$

4. Characterization of parameter space. This section will examine the system dynamics across the parameter space, and characterize the dynamics using the entropy and energy measures. The advantages and disadvantages of each measure will be assessed in their ability to capture the impact of changing γ and d. Then, phase plots of the parameter space will be presented and discussed. Finally, the solution behavior in different regimes will be visualized to show characteristics of different regimes.

4.1. Measures. A measure based on Shannon entropy S will be compared with the energy norm E, defined as follows:

$$s(x) = -\sum_{i,j} \hat{x}_{i,j} \log \hat{x}_{i,j},$$
$$e(x) = \|x\|_E = \|\nabla x\|_2 + \|x\|_2.$$

Here, $\hat{x}$ denotes a vector that sums to one, or the probability density form of x. When applied to solutions, both measures are expressed as the magnitude of the deviation from steady state,

$$S(u_t) = |s(u_t) - s(u_{ss})|,$$
$$E(u_t) = |e(u_t) - e(u_{ss})|.$$

4.2. Impact of γ and d. For each point $(\gamma, d) \in \mathcal{P}$, the entropy and energy measures were calculated for each state in the solution trajectory of u_1. The impact of reactivity γ is apparent in the time domain (Fig. 4.1 column 1), while the effect of the diffusion ratio d is clear in the frequency domain (Fig. 4.1 column 2).

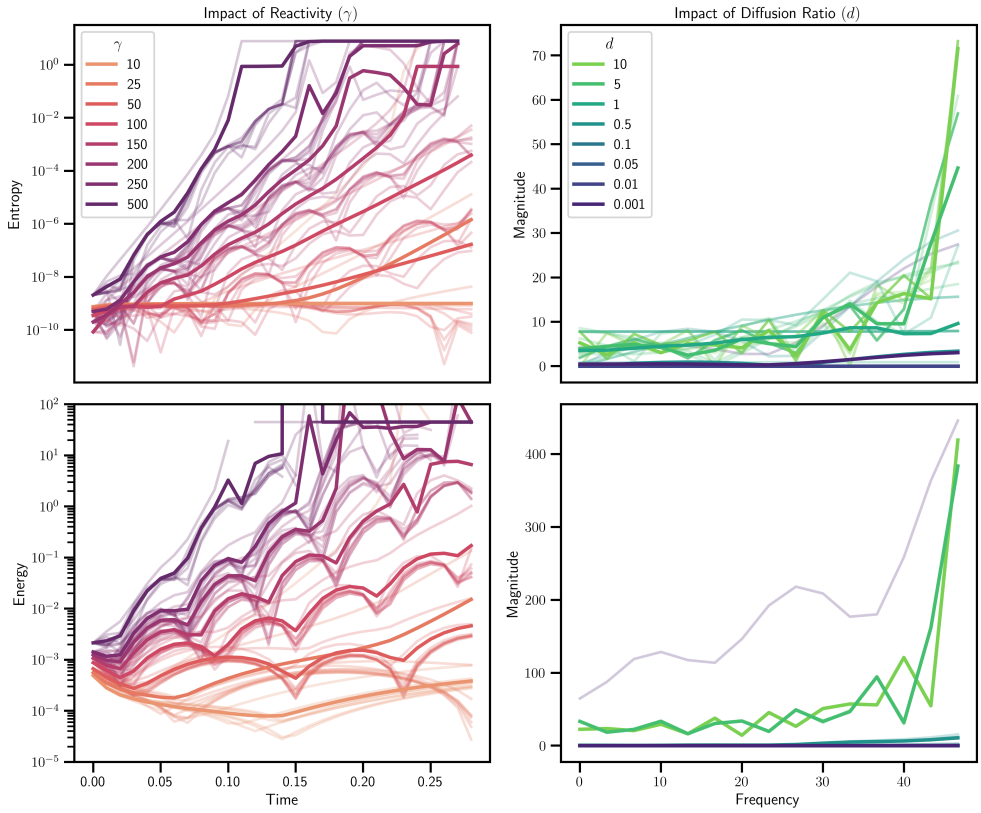

FIG. 4.1. *Time and frequency domain analysis of entropy and energy measures of u_1 for varying reactivity γ and diffusion ratio d. Left panels show the time evolution of the measures, and right panels display their frequency spectra. Average values are shown as bold lines, while individual trajectories are transparent.*

Across both measures, higher reactivity (γ) promotes divergence from steady state, reflecting increasing system disorder and more chaotic dynamics. The entropy measure shows a linear trend on the semi-log plot, indicating exponential growth away from steady state. This average behavior is smooth and systematic, but exhibits greater variance across diffusion ratios d for the same reactivity γ (indicated by spread out lines of the same color). Contrarily, the energy norm captures more nonlinear and oscillatory behavior. It also shows clearer grouping of trajectories for the same γ (closer groupings by color) suggesting the ability to separate the effect of γ from d.

In the frequency domain, both measures reveal that higher d values amplify the spectrum, particularly at higher frequencies. The entropy measure displays a gradual increase in frequency magnitude, with more variance in behavior for a specific d value. Opposite, the transition from low amplitude to higher amplitude is very sharp in the energy norm, with the highest two d values being clearly separate from the rest of the group. Like reactivity in the time domain, the energy norm has distinct grouping by d,

with variance so low that it is barely visible. Overall, the energy norm better separates the effects of γ and d, particularly in the frequency domain, while the entropy measure excels at capturing smooth, global trends, such as exponential divergence in the time domain and gradual spectral amplification in the frequency domain.

4.3. Phase plots. The two measures offer unique perspectives on the system's behavior across the parameter space, presented in Fig. 4.2a. In accordance with literature, entropy effectively captures a phase boundary by exhibiting a characteristic sharp gradient between two regimes [4]. In contrast, the energy norm displays smoother transitions between the stable (I) and diverging (III) regions. This smoother transition reflects subtleties in the dynamics, which may be influenced by the short time domain over which the problem was solved.

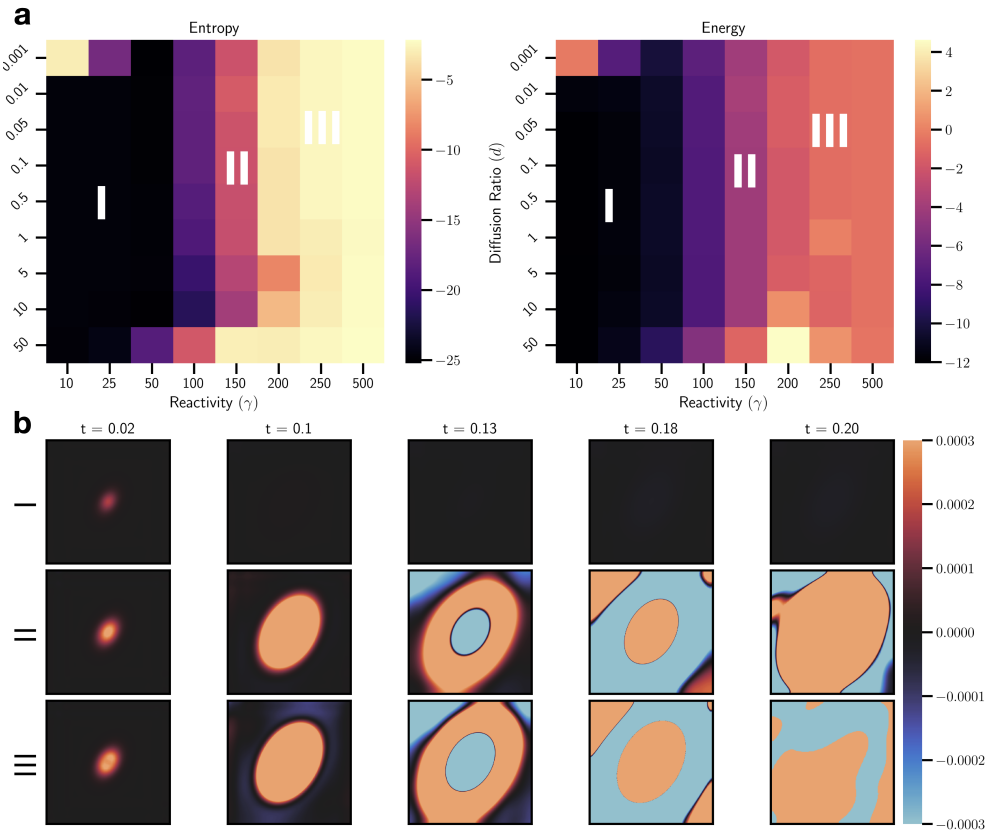

FIG. 4.2. ***(a)****Heatmap phase plots of the integrated energy and entropy measures for points* $(\gamma, d) \in \mathcal{P}$. ***(b)*** *Numerical solutions of* u_1 *for three representative points in the parameter space: I* $(\gamma = 10, d = 0.5)$*, II* $(\gamma = 150, d = 0.5)$*, and III* $(\gamma = 150, d = 0.1)$.

The difference in sensitivity to system behavior is the primary factor distinguishing factor between the energy and entropy phase plots. The entropy measure appears to detect divergence more quickly, identifying the phase regime with less time data before the system fully diverges. This suggests that entropy is well suited for identifying and dividing the parameter space into phases, while the energy norm captures subtle variations within phase regimes.

While the phase plots effectively highlight the impact of reactivity, they fail to communicate the influence of the diffusion ratio on the oscillatory behavior observed in Fig. 4.1. This suggests that the creation of phase plots by integrating the measures over time may suppress the impact of the diffusivity ratio. The effect of d may become more evident a wider section of the parameter space is explored, or if solutions are calculated for later time values. Alternatively, incorporating the frequency domain in the analysis could reveal the impact of d since its impact is on the spectra, with a less visible impact in the time domain.

Three points in parameter space $\{\mathrm{I} = (10, 0.5), \mathrm{II} = (150, 0.1), \mathrm{III} = (250, 0.05)\} \in \mathcal{P}$ are marked in Fig. 4.2a. The solutions for each of these points are visualized in Fig. 4.2b, illustrating the system's response under varying reactivity γ and diffusion ratio d. At the first point (I), where $\gamma = 10$ and $d = 0.5$, the perturbation from steady state is quickly smoothed by the diffusion dominated dynamics. The strong diffusion prevents the growth of spatial gradients, and the system quickly returns to steady state by $t = 0.1$. The solution represents a stable and smooth recovery to equilibrium steady state.

At the second point (II), where $\gamma = 150$ and $d = 0.1$, the system transitions to a chaotic state. The initial perturbation triggers the periodic generation of well-defined, ripple-like structures that expand symmetrically. This behavior arises from the pattern-forming nature of reaction-diffusion systems, where reactivity promotes spatial gradients while diffusion smooths them. Over time, the ripples amplify in both magnitude and spatial extent, increasing disorder until the system begins to diverge significantly from the steady state. The structured rings highlight a balance between diffusion and reactivity.

The third point (III), where $\gamma = 250$ and $d = 0.05$, has similar, yet accelerated dynamics compared to point II. The higher reactivity overwhelms the limited diffusive effects, leading to a rapid amplification of small perturbations. The periodic ripples grow in magnitude and propagate faster, eventually breaking down into large, irregular patterns. The dominance of reactivity in this regime drives the system into a chaotic and disordered state far more quickly, with diffusion unable to regulate the reactive forces.

5. Discussion. This study compared the effectiveness of the energy norm and a measure based on Shannon entropy in capturing the dynamic behavior of a coupled reaction diffusion system across a range of parameters. The analysis of time and frequency domains demonstrated that higher reactivity (γ) promotes system instability and divergence from equilibrium (steady state), while higher diffusion ratios (d) amplify magnitudes in the frequency domain in both the entropy and energy measures. On top of this commonality, each measure offered distinct and complementary information into how reactivity γ and diffusion ratio d influenced system behavior.

The entropy measure effectively identifies sharp transitions between phases, exhibiting a characteristic gradient that clearly delineates stable and unstable regions. Notably, entropy requires minimal time data to detect the onset of divergence, allowing the identification of phase boundaries in systems where time integration is computationally expensive. When viewed over time, the entropy measure exhibited smooth exponential growth with a rate dependent on γ in the time domain and a gradual amplification of spectral magnitude proportional to d in the frequency domain. In contrast, the energy norm captured more subtle variations in the phase plot, producing smoother transitions across the parameter space. When viewed over time, the energy norm is able to separate the independent effects of γ and d exhibiting a

clear grouping by each parameter in the time and frequency domain respectively.

However, there are limitations to this study. The patterns observed did not fully match prior results in [15], likely due to the inability to enforce no-flux boundary conditions due to the use of a linear basis. This limitation could be addressed by employing higher-order basis functions, which would allow higher-order derivative constraints to be enforced. Additionally, the assumption of boundedness for the reaction terms (R) for stability is likely violated at large times, as diverging solutions cannot remain bounded. These issues highlight the need for further investigation, particularly into long-term behavior and the implementation of boundary constraints.

These findings are significant for analyzing complex systems across science and engineering. In chemical systems, entropy can rapidly identify instabilities and phase transitions, serving as an efficient tool for predicting and preventing dangerous runaway reactions. In biological systems, where spatial patterns and oscillatory dynamics are critical, the energy norm provides detailed insights into how system parameters influence emergent behaviors. Furthermore, the two measures offer potential as tools for parameter estimation. By analyzing data in the energy or entropy domain – where the effects of parameters are isolated – identifying a system's location within the parameter space becomes more straightforward. Together, the energy and entropy measures provide a versatile framework for investigating a wide range of dynamical systems, including problems in reaction engineering, materials science, and biological pattern formation. While this study isolated the complementary effects of energy and entropy, measures of free energy combine these effects and are well studied in applications beyond thermodynamics [19, 20].

6. Conclusion. The results of this study illustrate the effectiveness of tools from statistical mechanics and thermodynamics in analyzing complex systems. Concepts such as energy, entropy, and parameters driving phase changes and emergent behavior provide a robust framework for understanding a coupled reaction diffusion problem. By comparing the energy norm and Shannon entropy, this work revealed their complementary roles: entropy excels at identifying phase boundaries and transitions, while energy isolates the more nuanced impact of system parameters on dynamics.

Here, the power of interdisciplinary approaches in advancing scientific understanding is clear. Borrowing tools from other disciplines has long been a driver of scientific innovation. This work highlights the advantages of interdisciplinary approaches, offering a framework to explore and expand the use of tools borrowed from statistical mechanics and thermodynamics in the study of dynamical systems.

Acknowledgments. The author expresses gratitude to the anonymous peer for their valuable feedback on the project proposal and to Professor Adler for his insightful guidance throughout the study. This project drew significant inspiration from Klishin et al.'s work, *Statistical Mechanics of Dynamical System Identification* [20].

REFERENCES

[1] Nigel Goldenfeld. *Lectures on Phase Transitions and the Renormalization Group*. Addison-Wesley, 1992.
[2] Herbert B. Callen. *Thermodynamics and an Introduction to Thermostatistics*. Wiley, 1985.
[3] Mehran Kardar. *Statistical Physics of Fields*. Cambridge University Press, 2007.
[4] M. C. Cross and P. C. Hohenberg. Pattern formation outside of equilibrium. *Reviews of Modern Physics*, 65(3):851, 1993.
[5] Claude E. Shannon. A mathematical theory of communication. *Bell System Technical Journal*, 27:379–423, 623–656, 1948.

[6] David J. C. MacKay. *Information Theory, Inference, and Learning Algorithms*. Cambridge University Press, 2003.

[7] K. J. George and R. I. Sujith. Disturbance energy norms: A critical analysis. *Journal of Sound and Vibration*, 2012.

[8] M. V. Pham, M. N. Nguyen, and T. Q. Bui. Numerical simulation of localized quasi-brittle fracture with an enhanced bi-energy norm based equivalent strain. *Engineering Fracture Mechanics*, 2023.

[9] J. C. Simo and J. W. Ju. Strain-and stress-based continuum damage models—i. formulation. *International Journal of Solids and Structures*, 1987.

[10] L. E. Garcia-Castillo, D. Pardo, and I. Gomez-Revuelto. A two-dimensional self-adaptive hp finite element method for the characterization of waveguide discontinuities. part i: Energy-norm based automatic hp-adaptivity. *Computer Methods in Applied Mechanics and Engineering*, 2007.

[11] J. D. Murray. *Mathematical Biology II: Spatial Models and Biomedical Applications*. Springer, 2003.

[12] Alan Turing. The chemical basis for morphogenesis. *Philosophical Transactions of the Royal Society B*, 1952.

[13] Fatemeh Shakeri and Mehdi Dehghan. The finite volume spectral element method to solve turing models in the biological pattern formation. *Computers and Mathematics with Applications*, 2011.

[14] S.A. Newman M. Alber J. Zhu, Y.-T. Zhang. Application of discontinuous galerkin methods for reaction–diffusion systems in developmental biology. *Journal of Scientific Computing*, 2009.

[15] J.G. Verwer W. Hundsdorfer. Numerical solution of time-dependent advection–diffusion–reaction equations. *Springer, Berlin*, 2003.

[16] Kendall E. Atkinson. *An Introduction to Numerical Analysis*. Wiley, 2nd edition, 1989.

[17] Nathan Bell, Luke N. Olson, and Jacob Schroder. Pyamg: Algebraic multigrid solvers in python. *Journal of Open Source Software*, 2024.

[18] Scott MacLachlan James Adler, Hans De Sterck and Luke Olson. *Numerical Partial Differential Equations*. N/A, preprint edition, 2024.

[19] Karl Friston, Lancelot Da Costa, Noor Sajid, Conor Heins, Kai Ueltzhöffer, Grigorios A. Pavliotis, and Thomas Parr. The free energy principle made simpler but not too simple. *Physics Reports*, 1024:1–29, 2023. The free energy principle made simpler but not too simple.

[20] Andrei A. Klishin, Joseph Bakarji, J. Nathan Kutz, and Krithika Manohar. Statistical mechanics of dynamical system identification, 2024.